The oceanic response to mesoscale atmospheric forcing

Thomas Jung[1], Soumia Serrar[1], and Qiang Wang[1]

[1] Alfred Wegener Institute, Helmholtz Centre for Polar and Marine Research, Bremerhaven, Germany

Abstract The response of the oceanic circulation to mesoscale atmospheric forcing is studied by comparing integrations of a global sea ice-ocean model with high-resolution European Centre for Medium-Range Weather Forecasts analysis data (0.4°) to those with the same forcing coarse grained to a resolution typically employed in climate models and atmospheric reanalyses (1.8°). It is shown that the representation of mesoscale features in atmospheric forcing fields leads to an increase in the strength of the wind-driven gyres in the North Atlantic and North Pacific regions of about 5–10% of its mean value. An increase of similar magnitude is found for the Atlantic meridional overturning circulation. From the results of this study it is argued that small-scale atmospheric phenomena such as fronts, mesoscale cyclones, and topographic jets play an important role in driving the mean oceanic circulation.

1. Introduction

The oceanic response to atmospheric forcing has been the subject of extensive research for many decades [e.g., *Bjerknes*, 1964; *Frankignoul*, 1985; *Eden and Jung*, 2001], and it is now widely accepted that the large-scale ocean circulation is strongly driven by the overlying atmosphere, both in terms of its mean state and variability. From the wide range of atmospheric scales the emphasis of previous studies has been on larger synoptic and especially planetary scales.

Partly fueled by the availability of increased supercomputing resources and high-resolution observational and analysis products, the influence of mesoscale atmospheric phenomena [*Chelton et al.*, 2004] on the ocean circulation has become a topic of more intensive research. *Pickart et al.* [2003], for example, suggest that deep water formation in the southwest Irminger Sea is the direct result of the presence of strong topographically forced Greenland tip jet events [*Doyle and Shapiro*, 1999] that are associated with enhanced oceanic heat loss and wind stress curl. Operational high-resolution atmospheric analysis fields have been used by *Eden and Jung* [2006] to force a global ocean model. By comparing the results with the high-resolution forcing to that with climatological forcing, they detected an increased activity of ocean eddies, and hence, plankton blooms in the wake of mountainous islands in the trade wind regions. More recently, still *Condron et al.* [2008] and *Condron and Renfrew* [2013] have shown that increased wind speed and turbulent heat fluxes in mesoscale polar lows lead to increases in the simulated depth, frequency, and area of deep convection in the Nordic Seas, which in turn leads to a larger northward transport of heat into the region.

While the influence of atmospheric mesoscale phenomena has been investigated previously [see also *Tokmakian*, 2005; *Sasaki et al.*, 2006; *Haine et al.*, 2009], this study can be seen as a substantial step forward since the pure effect of resolution is isolated by employing a coarse-graining approach. Furthermore, the use of global forcing fields in a global modeling framework allows for a more complete assessment than available from previous studies.

2. Methods

To study the influence of small-scale atmospheric structures on the ocean circulation, experiments with the global finite element sea ice-ocean model (FESOM) are carried out. The dynamic-thermodynamic sea ice module is based on the model formulation of *Parkinson and Washington* [1979] and *Hunke and Dukowicz* [2001]. FESOM is the first global model of its kind that employs an unstructured mesh approach [*Danilov et al.*, 2004; *Wang et al.*, 2008; *Timmermann et al.*, 2009].

In the configuration used here a nominal horizontal resolution of about 1° is used for the bulk of the open ocean; along the coastlines the resolution is doubled to about 0.5°. A further refinement to about
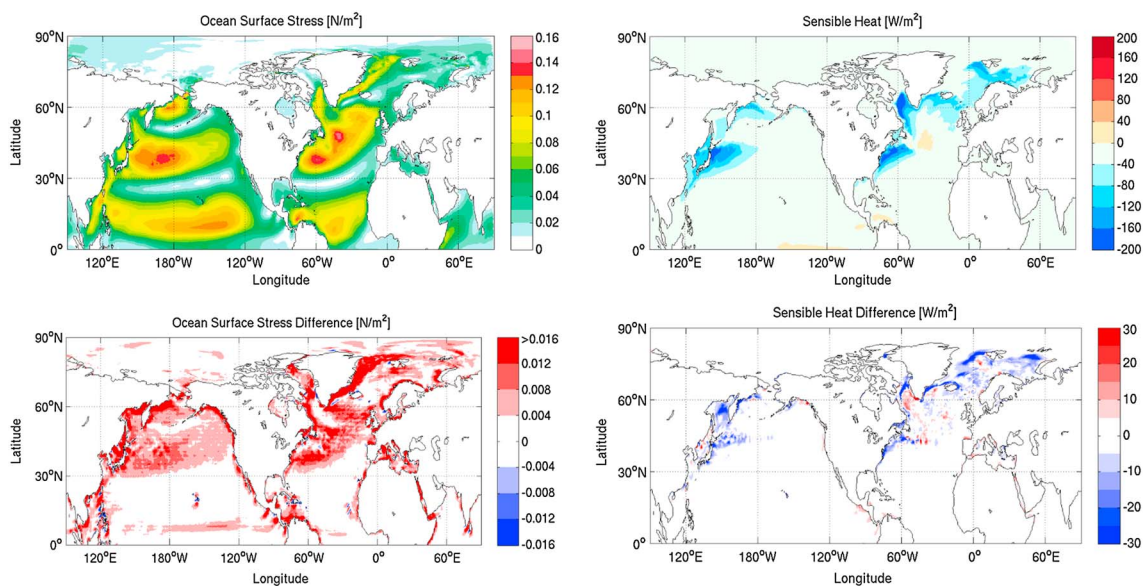
Figure 1. Climatological (top left) magnitude of turbulent surface wind stress (N m^{-2}) and (top right) turbulent sensible heat flux (W m^{-2}) during wintertime (JFM) obtained from the experiment with low-resolution atmospheric forcing. Also shown are the mean differences between the experiments with high-resolution and low-resolution atmospheric forcing for (bottom left) turbulent wind stress (N m^{-2}) and (bottom right) turbulent sensible heat flux (W m^{-2}). Results are shown on the model grid.

24 km (9 km) is used north of 50°N (in the subpolar North Atlantic and the Nordic Seas). In the vertical, the mesh has 46 z levels with a thickness of 10 m in the top 100 m that is gradually increasing downward. The ocean is initialized with temperature and salinity fields from PHC3 climatology [*Steele et al.*, 2001] and the sea ice with average fields obtained from a 20 year model simulation with a prescribed annual cycle of atmospheric forcing.
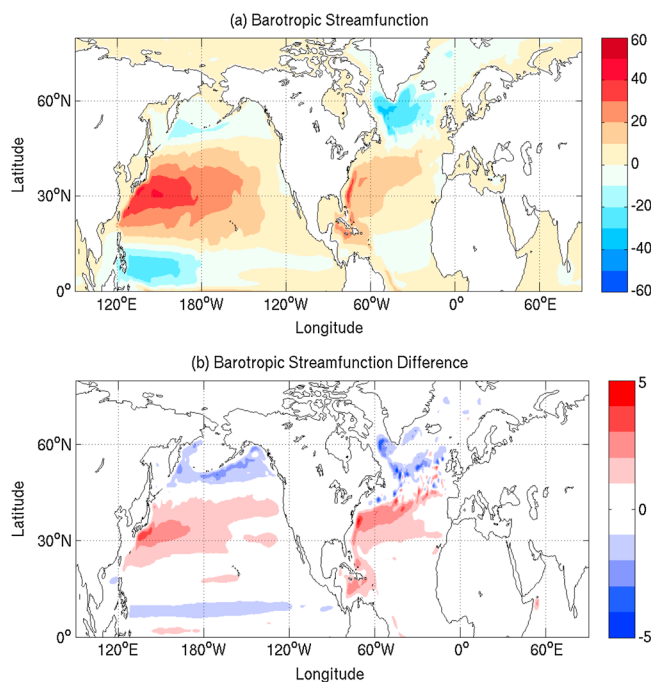

Figure 2. (a) Climatological mean barotropic stream function (Sv, $1Sv = 10^6$ m^3's^{-1}) for the experiment with low-resolution atmospheric forcing and (b) the mean difference of the barotropic stream function (Sv) between the experiment with high-resolution and low-resolution atmospheric forcing. The average is taken over the last 20 years of the integration.

The atmospheric data (wind, temperature, humidity, and precipitation) were taken from the operational European Centre for Medium-Range Weather Forecasts (ECMWF) analysis for the period 2001 to 2010. During the period 2001–2004 a resolution of approximately 40 km is available; horizontal resolution was increased to 25 km and 12 km on 6 January 2005 and 26 January 2010, respectively. While the operational analysis lacks the homogeneity provided by reanalysis efforts, it provides a resolution that goes well beyond most available reanalysis products. The 6-hourly turbulent surface heat and momentum fluxes as well as radiative fluxes used to force the model were computed by applying bulk formulae to the parameters from the ECMWF analysis and the ocean model (SST and surface velocity). Precipitation was obtained directly from corresponding 6-hourly forecasts with the ECMWF model.

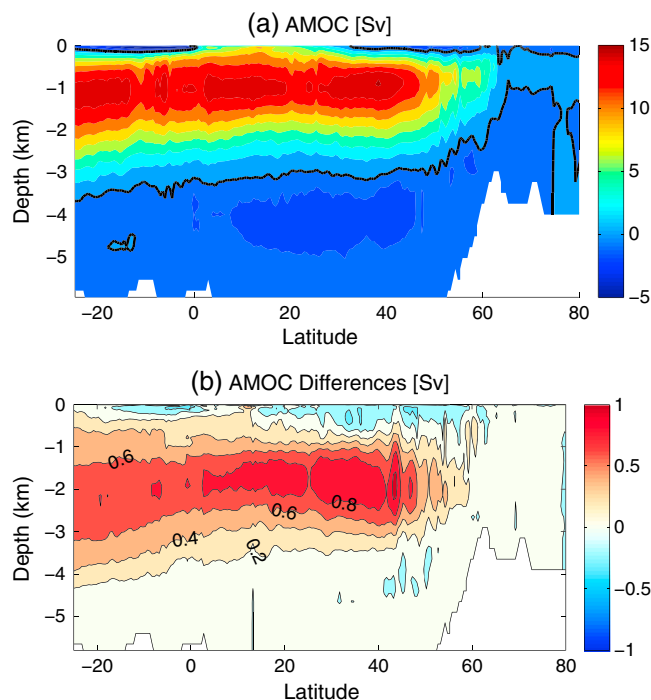In order to isolate the influence of mesoscale atmospheric

Figure 3. Same as in Figure 2, except for the Atlantic Meridional Overturning Circulation (in *Sv*) as a function of depth and latitude.

phenomena, two sets of model experiments were carried out. In the first 40 year experiment the high-resolution forcing, interpolated to the joint resolution of about 0.4°, was repeatedly applied four consecutive times. The same approach was used in the second experiment with the difference that the ECMWF data was coarse grained to a horizontal resolution of about 1.8° prior to the computation of the surface fluxes. Coarse graining was achieved by area averaging all grid points from the high-resolution mesh lying in each of the grid cells of the low-resolution mesh. By considering the difference between the two experiments for the last 20 years of the integrations (i.e., after the model has adjusted to the new forcing), it is possible to isolate the influence of mesoscale atmospheric phenomena.

3. Results

To start with, it is worth considering the influence of small-scale atmospheric features on turbulent flux fields at the air-sea interface that are used to drive the sea ice-ocean model. Figure 1 reveals that the mean magnitude of turbulent surface momentum fluxes (τ hereafter) increases with enhanced atmospheric resolution. This can be explained by the nonlinear dependence of the wind stress on wind itself (the mean wind components remain unchanged, not shown). Decreased values of τ are only found in very localized areas most of which lie in vicinity of topographic features such as the Cape Verdes islands. The spatial pattern of the increase of τ resembles the climatological mean field suggesting that the use of high-resolution atmospheric forcing leads to an increase in the climatological wind-driven oceanic circulation. Over the open ocean along the Gulf Stream and North Atlantic current, where the main North Atlantic storm tracked is situated, the increase in τ amounts to about 10% of the climatological mean. The wind stress associated with the North Atlantic trade winds, however, remains largely unchanged due to their steady and relatively large scale nature. In coastal areas the largest differences are found (up to 50%) such as along the eastern coast of Greenland where "barrier winds" are known to be prevalent [*Harden et al.*, 2011] which are not well resolved at 1.8° resolution [*Petersen et al.*, 2009; *Renfrew et al.*, 2009].

Climatological turbulent sensible heat fluxes (F_{SH} hereafter) with low-resolution atmospheric forcing are also shown in Figure 1 along with the changes of F_{SH} when mesoscale atmospheric phenomena are incorporated in the forcing. The low-resolution fields show the well-known loss of sensible heat in the Gulf Stream and Kuroshio [e.g., *Gulev et al.*, 2007]. Furthermore, sensible heat is lost to the atmosphere in the northeastern North Atlantic, in the Bering Sea, Labrador Sea, as well as in the Nordic Seas. Increased resolution of the atmospheric forcing leads to increased F_{SH} due to enhanced wind speed in the Gulf Stream and Kuroshio region and due to sharper sea ice edges in the high latitudes. Like for τ, incorporating mesoscale phenomena in the atmospheric forcing tends to enhance climatological turbulent sensible heat fluxes from the ocean to the atmosphere.

The climatological mean barotropic stream function as simulated by FESOM with the low-resolution forcing is shown in Figure 2 together with the response to incorporating mesoscale atmospheric phenomena in the forcing. As expected from the wind stress fields, the wind-driven horizontal barotropic circulation in the North Atlantic and North Pacific increased by about 10%. This increase is statistically significant at the 95% confidence level using a Student's *t* test taking serial correlation into account (not shown). The subtropical
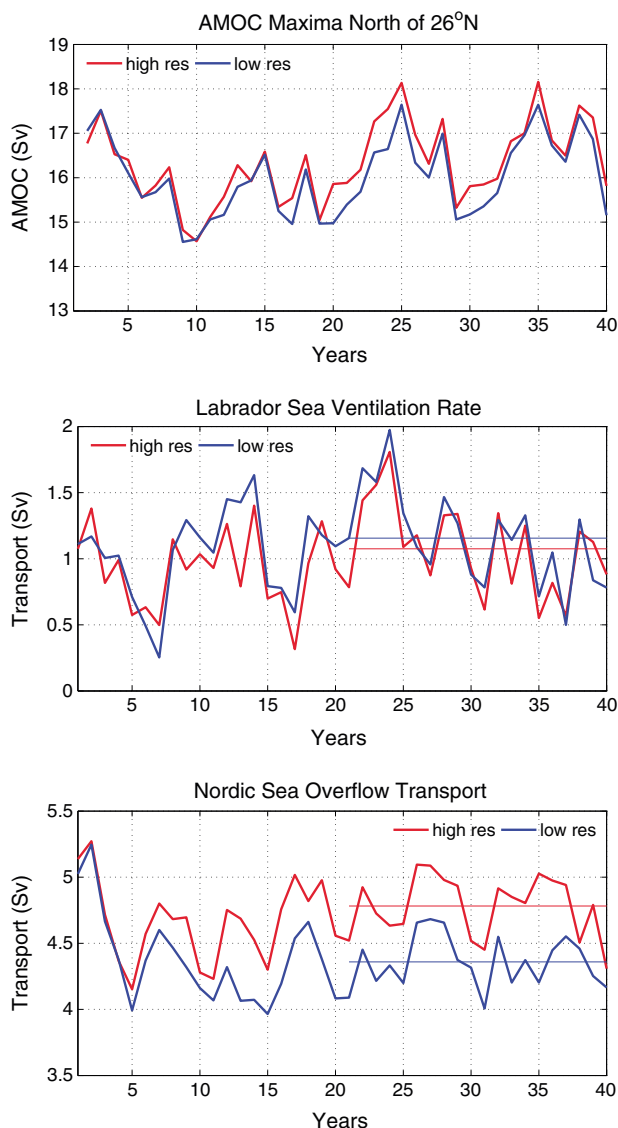
Figure 4. Time series of (top) the maximum Atlantic Meridional Overturning circulation north of 26°N, (middle) the Labrador Sea Water ventilation rate (LSW in *Sv*) and (bottom) the Nordic Sea Overflow transport (NSO in *Sv*) for the experiment with low-resolution (blue) and high-resolution (red) forcing. LSW is calculated as the difference of Labrador Sea Water (27.74 kg/m^3 < σ_θ < 27.8 kg/m^3) transport between the outflow at 53°N and the inflow near the southern tip of Greenland. The NSO transport is calculated for water masses of σ_θ > 27.8 kg/m^3 at the Greenland-Scotland Ridge. Notice that the same atmospheric forcing from the period 2001–2010 has been applied repeatedly for four times.

response on the eastern sides of the ocean is less pronounced. This is in line with the fact that the wind stress associated with the trade winds is sufficiently well described by the coarser resolution forcing.

In the experiment with high-resolution atmospheric forcing there is also an increase in the strength of the Antarctic Circumpolar Current of about 5–10% which is consistent with an increase in the climatological mean wind stress over the Southern Ocean (not shown).

The simulated mean Atlantic meridional overturning circulation (AMOC) for the experiment with low-resolution atmospheric forcing is shown in Figure 3a. The simulated AMOC resembles that of other sea ice-ocean models with a maximum strength of about 15 *Sv* and a second cell in the deep ocean. Like many other models, the AMOC in FESOM appears to be weaker than observational estimates [*Danabasoglu et al.*, 2014]. By using high-resolution atmospheric forcing, the AMOC strengthens slightly (about 5–10%) and its maximum shifts downward (Figure 3b).

Time series of the maximum AMOC north of 26° for the two experiments show that the oceanic response to the high-resolution forcing takes a few years to develop (Figure 4). After 10–20 years the AMOC is consistently stronger in the experiment with high-resolution forcing. A more detailed analysis of the oceanic changes shows that the Labrador Sea Water ventilation rate does not increase for the experiment with high-resolution atmospheric forcing (Figure 4); rather increases in overflow waters (Figure 4) seem to be responsible for the enhanced strength of the AMOC. Both the increase in the AMOC and in the overflow, with equal contributions from Denmark Strait and Faroe-Shetland Channel (not shown), are statistically significant at the 95% confidence level (two-sided Student's *t* test taking serial correlation into account).

4. Discussion

Based on numerical experimentation with realistic high-resolution atmospheric forcing fields and a coarse-grained counterpart, it is shown that small-scale atmospheric phenomena such as fronts, mesoscale cyclones, and topographic jets collectively lead to a strengthening of the mean horizontal wind-driven

ocean circulation of about 5–10%. Furthermore, a slight strengthening of the AMOC is found whose origin appears to lie in turbulent surface heat flux changes in the Nordic Seas.

In terms of magnitude, the oceanic response described here is comparable to what has been found previously in other sensitivity experiments (e.g., changes in certain model parameters). However, we would argue that the influence of atmospheric mesoscale features on the ocean circulation described in this study is special due to its *systematic* nature, which can be explained by the strongly nonlinear dependence of turbulent surface fluxes on atmospheric and oceanic parameters.

The mean oceanic response to mesoscale atmospheric forcing described here is substantial given that relatively little atmospheric kinetic energy resides in the mesoscale [*Nastrom and Gage*, 1985; *Gulev et al.*, 2002]. This raises the question as to how synoptic-scale atmospheric motions, which are much more energetic, influence the ocean circulation. The coarse-graining approach employed in this study could help to provide an answer to this question.

The high-resolution atmospheric forcing from the operational ECMWF analysis used in this study is not readily available, and it is more prone to inhomogeneities than reanalysis data. While we do not think that inhomogeneities influence the conclusions of this study, it is promising to see that reanalysis projects are moving to increasingly high spatial resolution [*Saha et al.*, 2010]. The availability of high-resolution reanalysis products will help to explore the role of mesoscale atmospheric phenomena in more detail, especially in terms of climate variability and climate change.

The results presented in this study suggest that the relatively coarse atmospheric resolution typically used in CMIP5 models will lead to an underestimation of the AMOC and wind-driven circulation. In fact, the results presented in this study are presumably still rather conservative given that a coarse-grained high-resolution atmospheric model will capture more variability than a model that has been actually run at coarse resolution [*Skamarock*, 2004; *Jung et al.*, 2012; *Kinter et al.*, 2013]. In order to substantiate this hypothesis, 1 day forecasts have been run with the ECMWF model for each day of the winter December 2011 to February 2012 at two different horizontal resolutions (1.8° and 0.4°) (see also *Jung and Rhines* [2007], for an application of this approach). While the spatial structure of the mean turbulent flux differences is very similar to the one obtained by coarse graining the high-resolution analysis data, the magnitude of the difference is significantly higher, locally up to factor of 2 and more, when the model is run at different horizontal resolutions (not shown). This supports the notion that the oceanic response to mesoscale atmospheric forcing reported here is a rather conservative estimate.

References

Bjerknes, J. (1964), Atlantic air-sea interaction, *Adv. Geophys.*, *10*, 1–82.
Chelton, D. B., M. G. Schlax, M. H. Freilich, and R. F. Milliff (2004), Satellite measurements reveal persistent small-scale features in ocean winds, *Science*, *303*, 978–983.
Condron, A., and I. A. Renfrew (2013), The impact of polar mesoscale storms on northeast Atlantic Ocean circulation, *Nat. Geosci.*, *6*, 34–37.
Condron, A., G. R. Bigg, and I. A. Renfrew (2008), Modeling the impact of polar mesocyclones on ocean circulation, *J. Geophys. Res.*, *113*, C10005, doi:10.1029/2007JC004599.
Danabasoglu, G., et al. (2014), North Atlantic simulations in coordinated ocean-ice reference experiments phase II. Part I: Mean states, *Ocean Model.*, *73*, 76–107.
Danilov, S., G. Kivman, and J. Schröter (2004), A finite-element ocean model: Principles and evaluation, *Ocean Model.*, *6*, 125–150.
Doyle, J. D., and M. A. Shapiro (1999), Flow response to large-scale topography: The Greenland tip jet, *Tellus*, *51*, 728–748.
Eden, C., and T. Jung (2001), North Atlantic interdecadal variability: Oceanic response to the North Atlantic Oscillation (1865–1997), *J. Clim.*, *14*, 676–691.
Eden, C., and T. Jung (2006), Wind-driven eddies and plankton blooms in the North Atlantic ocean, *Technical Memorandum 460*, ECMWF, Shinfield Park, Reading, Berkshire RG2 9AX, U. K.
Frankignoul, C. (1985), Sea surface temperature anomalies, planetary waves, and air-sea feedback in the middle latitudes, *Rev. Geophys.*, *23*, 357–390.
Gulev, S., T. Jung, and E. Ruprecht (2007), Estimation of the impact of sampling errors in the VOS observations on air-sea fluxes. Part I: Uncertainties in climate means, *J. Clim.*, *20*, 279–301.
Gulev, S. K., T. Jung, and E. Ruprecht (2002), Climatology and interannual variability in the intensity of synoptic-scale processes in the North Atlantic from the NCEP/NCAR reanalysis data, *J. Clim.*, *15*, 809–828.
Haine, T., S. Zhang, G. Moore, and I. Renfrew (2009), On the impact of high-resolution, high-frequency meteorological forcing on Denmark Strait ocean circulation, *Q. J. R. Meteorol. Soc.*, *135*, 2067–2085.
Harden, B. E., I. A. Renfrew, and G. N. Petersen (2011), A climatology of wintertime barrier winds off southeast Greenland, *J. Clim.*, *24*, 4701–4717.
Hunke, E., and J. Dukowicz (2001), The elastic-viscous-plastic sea ice dynamics model in general orthogonal curvilinear coordinates on a sphere-incorporation of metric term, *Mon. Weather Rev.*, *130*, 1848–1865.
Jung, T., and P. B. Rhines (2007), Greenland's pressure drag and the Atlantic storm track, *J. Atmos. Sci.*, *64*, 4004–4030.

Jung, T., et al. (2012), High-resolution global climate simulations with the ECMWF model in Project Athena: Experimental design, model climate, and seasonal forecast skill, *J. Clim.*, *25*, 3155–3172.

Kinter, J., et al. (2013), Revolutionizing climate modelling with Project Athena: A multi-institutional, international collaboration, *Bull. Am. Meteorol. Soc.*, *94*, 231–245.

Nastrom, G., and K. S. Gage (1985), A climatology of atmospheric wavenumber spectra of wind and temperature observed by commercial aircraft, *J. Atmos. Sci.*, *42*(9), 950–960.

Parkinson, C., and W. Washington (1979), A large-scale numerical model of sea ice, *J. Geophys. Res.*, *84*, 311–337.

Petersen, G., I. Renfrew, and G. Moore (2009), An overview of barrier winds off southeastern Greenland during GFDex, *Q. J. R. Meteorol. Soc.*, *135*, 1950–1967.

Pickart, R. S., M. A. Spall, M. H. Ribergaard, G. W. K. Moore, and R. F. Milliff (2003), Deep convection in the Irminger Sea forced by the Greenland tip jet, *Nature*, *424*, 152–156.

Renfrew, I., G. Petersen, D. Sproson, G. Moore, H. Adiwidjaja, S. Zhang, and R. North (2009), A comparison of aircraft-based surface-layer observations over Denmark Strait and the Irminger Sea with meteorological analyses and QuikSCAT winds, *Q. J. R. Meteorol. Soc.*, *135*, 2046–2066.

Saha, S., et al. (2010), The NCEP climate forecast system reanalysis, *Bull. Am. Meteorol. Soc.*, *81*, 1015–1057.

Sasaki, H., Y. Sasai, M. Nonaka, Y. Masumoto, and S. Kawahara (2006), An eddy-resolving simulation of the quasi-global ocean driven by satellite-observed wind field: Preliminary outcomes from physical and biological fields, *J. Earth Simulator*, *6*, 35–49.

Skamarock, W. (2004), Evaluating mesoscale NWP models using kinetic energy spectra, *Mon. Weather Rev.*, *132*, 3019–3032.

Steele, M., R. Morley, and W. Ermold (2001), PHC: A global ocean hydrography with a high-quality Arctic Ocean, *J. Clim.*, *14*, 2079–2087.

Timmermann, R., S. Danilov, J. Schröter, C. Böning, D. Sidorenko, and K. Rollenhagen (2009), Ocean circulation and sea ice distribution in a finite element global sea ice–ocean model, *Ocean Model.*, *27*, 114–129.

Tokmakian, R. (2005), An ocean model's response to scatterometer winds, *Ocean Model.*, *9*, 89–103.

Wang, Q., S. Danilov, and J. Schröter (2008), Finite element ocean circulation model based on triangular prismatic elements, with application in studying the effect of topography representation, *J. Geophys. Res.*, *113*, 1978–2012, doi:10.1029/2007JC004482.